RSC Advances

PAPER

View Article Online
View Journal | View Issue

Cite this: *RSC Adv.*, 2024, **14**, 12107

Label-free detection of Aβ-42: a liquid crystal droplet approach for Alzheimer's disease diagnosis

Saumya Ranjan Pradhan,[a] Ramadevi Suguru Pathinti,[a] Ramesh Kandimalla,[b] Krishnakanth Chithari,[a] Madhava Rao Veeramalla N.[c] and Jayalakshmi Vallamkondu *[a]

This study introduces a biosensor based on liquid crystals (LC) designed to detect the Aβ-42 biomarker, commonly associated with Alzheimer's disease. The sensor utilizes LC droplets created using a PEI/Tween-20 surfactant mixture, arranged radially in an aqueous solution. These droplets are coated with the Aβ1–16 antibody, enabling the detection of the Aβ1–42 biomarker. The key advantage of this biosensor lies in its ability to directly translate the antigen–antibody interaction into a change in the molecular orientation of the LC droplets, simplifying the detection process by removing additional procedural steps. Specifically, this immunoassay induces a transformation in the nematic droplets orientation from radial to bipolar upon successful antigen binding. When only the Aβ1–16 antibody coated the LC droplets, no change in orientation was detected, confirming the reaction's specificity. The orientation shift in the LC droplets indicates the formation of an immunocomplex between the Aβ1–16 antibody and the Aβ1–42 antigen. The LC droplet immunoassay effectively detected Aβ1–42 antigen concentrations ranging from 45 to 112.5 μM, with the Aβ1–16 antibody immobilized on the droplets at a concentration of 1 μg mL^{-1}. These findings suggest that the LC microdroplets' orientational behavior can be harnessed to develop a biosensor for the *in vivo* detection of various proteins or pathogens in a PBS aqueous medium. Owing to its label-free nature and distinct optical signaling, this LC droplet-based immunoassay holds promise for further development into a cost-effective, portable diagnostic tool.

Received 24th January 2024
Accepted 9th April 2024

DOI: 10.1039/d4ra00615a

rsc.li/rsc-advances

1. Introduction

Alzheimer's disease (AD), a progressive neurodegenerative disorder, is defined by alterations in brain structure and function that ultimately result in the buildup of specific protein deposits, posing a significant challenge to global healthcare systems. It is the most common cause of dementia, a general term for memory loss and other cognitive abilities serious enough to interfere with daily life. AD can easily be curable if it is identified at early stages.[1] In this regrading in medical different techniques as follows positron emission tomography (PET) and magnetic resonance imaging (MRI) are new techniques for detecting Alzheimer's disease.[2] In this technique diagnosis is only achievable after the illness has advanced, this procedure is both expensive and not easily available in all medicals, that is the last stage, which is impossible to cure and tough to treat. Biomarkers play a pivotal role in this context, offering a means to identify the disease before clinical symptoms become apparent. Many studies have demonstrated that AD may be diagnosed by evaluating quantitative biomarkers like as Aβ40, Aβ42, T-tau, and P-tau181.[3–7]

Among these biomarkers, the peptide Aβ-42 has gained prominence due to its strong association with the pathological mechanisms of AD. The amyloid beta fragment is a normal product of metabolism of amyloid protein, which is a transmembrane protein found in neuronal and glial cells of the brain.[8] Hence, for the diagnosis and prognosis of AD, Aβ-42 and its aggregates are regarded as potentially significant biomarkers in plasma and cerebral spinal fluid.[9–12] The detection of Aβ-42 in biological samples could provide a critical tool for early diagnosis, potentially leading to better patient outcomes.[3,13–15]

In recent years, a plethora of techniques for the early detection of AD has been developed. These include enzyme-linked immunoassay (ELISA),[16] optical imaging,[17] mass spectrometry,[18,19] fluorescence spectroscopy,[20] various electrochemical methods,[7] electrochemical impedance spectroscopy,[21–23] Raman spectroscopy,[24] plasmonic-based sensors,[25] and immunomagnetic reduction-based sensors.[26,27] Each of these methods has shown promise in effectively detecting the Aβ1–42 biomarker, which is crucial in Alzheimer's disease diagnosis. However, a significant limitation of these

[a]*Department of Physics, National Institute of Technology, Warangal 506004, India. E-mail: srpradhan8260@gmail.com; ramaphy@student.nitw.ac.in; chitharikrishnakanth2@gmail.com; jayalakshmiv@nitw.ac.in*

[b]*Department of Biochemistry, Kakatiya Medical College, Warangal 506007, India. E-mail: ramesh.kandimalla@gmail.com*

[c]*Department of Neurology, Gandhi Medical College, Secunderabad, 500003, India. E-mail: veeramalla_madhavarao@yahoo.com*

advanced methods is their cost, which can be prohibitively high for widespread use. Additionally, while these modern techniques offer improved detection capabilities, they often come with increased complexity and expense. Historically, ELISA has been the standard approach for antigen detection. Despite its widespread use, the preparation of reagents and the procedural intricacies involved in various ELISA methods can be quite complex and time-consuming.[28] This complexity further contributes to the overall challenges faced in the cost-effective and efficient detection of AD biomarkers.

LC-based biosensors have recently garnered attention due to their unique properties.[29–35] LCs, substances that exhibit a phase between solid and liquid, respond sensitively to external stimuli, including temperature, electric fields, and molecular interactions. This sensitivity can be exploited in biosensing applications, where the orientation of LC molecules changes in response to specific biomolecular interactions. This change in orientation can be observed optically, providing a simple yet effective way to detect the presence of target biomolecules. The use of LCs in biosensors, therefore, offers a promising avenue for the development of new diagnostic tools. The integration of LC technology into immunoassays for Alzheimer's biomarker detection presents several advantages. Traditional immunoassays often require elaborate procedures, including the use of labels or secondary agents, to produce a detectable signal. In contrast, LC-based immunoassays can transduce biomolecular interactions directly into optical signals through changes in the LC orientation. This label-free approach simplifies the assay process, potentially reducing costs and time. Moreover, the visual nature of the LC response facilitates easy and rapid detection, an essential feature for clinical diagnostics.[29–35]

LCs, owing to their anisotropic properties, have emerged as versatile tools in biosensing applications for detecting a range of biological entities, including various enzymes, bacteria,[36] viruses,[37] proteins,[38] and other biological particles.[39,40] The specificity in biosensing, particularly in the context of amyloid beta 1–42 detection, is often achieved by immobilizing a corresponding antibody on the LC surface.[41] Previous studies, such as those by Ipsita *et al.*, have demonstrated the efficacy of LCs in differentiating between various amyloid beta oligomers based on their conformational differences.[42] Furthermore, research by Emine *et al.* has detailed the development of a liquid crystal sensor capable of detecting varying concentrations of the Aβ1–42 peptide, evidenced through changes in sensor intensity.[43] Sohrabnavi *et al.* have developed LC-based biosensor for the early detection of Alzheimer's by measuring amyloid beta-42 concentration in human serum based on liquid crystal.[44] To our knowledge, there have been not many reports of amyloid beta 1–42 detection using nematic liquid crystal (NLC) droplets. LC microdroplets are particularly advantageous in biosensing for the detection of small analytes in aqueous solutions due to their large surface area.[45–53] The interfacial area of LC molecules in microdroplets is considerably greater compared to the same volume of LC molecules on confined planar surfaces, enhancing their sensitivity. These droplets are characterized by well-defined and tunable optical properties, which contribute to their increased sensitivity and selectivity towards various analytes. The size of the LC droplets plays a critical role in the biosensing efficiency; smaller droplet sizes generally lead to improved sensitivity.[52] In LC droplet biosensing, two primary sensing mechanisms are predominantly utilized: electrostatic interactions between the LC surfaces and biomolecules, and the immunoassay approach involving antibody–antigen (ligand–receptor) interactions.[41,43] These mechanisms have been successfully applied in the sensing of proteins, bacteria, viruses, bile acids, and disease detection, showcasing the versatility and efficacy of LC droplet-based biosensing technologies.[36–39]

In this study, we have engineered LC droplets by coating them with a mixture of polyethyleneimine (PEI) and Tween-20 surfactant, followed by immobilizing anti-beta amyloid 1–16 antibodies on the surface of these droplets. This configuration was developed specifically for the detection of the AD biomarker Aβ1–42. The stability of the LC droplets is ensured by the PEI/Tween-20 surfactant layer. Previously, our research group successfully employed LC droplets stabilized with polyvinyl alcohol (PVA)/SC12S for the detection of bile acids and bovine serum albumin (BSA), demonstrating a straightforward and cost-effective approach.[51,52] The PEI/Tween-20 stabilized LC droplets have been adapted for the detection of the Aβ1–42 biomarker. The detection methodology is predicated on the dynamic structural alterations in the LC droplets induced by the immunobinding reaction between the anti-Aβ1–16 and the Aβ1–42 antigen. This interaction disrupts the molecular alignment on the surface of the LC droplets, resulting in a transition from a radial to a bipolar configuration in the NLC droplets. We detect the antigen Aβ1–42 by identifying these structural changes from a hedgehog (radial) to boojums (bipolar) configuration in the antibody-immobilized LC droplets, observed under a polarizing optical microscope (POM) in transmission mode. Further, we investigated how the immobilization of anti-Aβ1–16 and the concentration of the Aβ1–42 peptide in a phosphate-buffered saline (PBS) solution influenced the responsive behaviour of the immobilized PEI/Tween-20 stabilized NLC droplets. To enhance our understanding of the anti-Aβ1–16 immobilization, we introduced a fluorescently labeled secondary antibody (anti-mouse IgG(H + L) F(ab′)2) to the antibody-antigen immunobinding reaction in the LC droplets and observed the outcomes under a fluorescence microscope. The NLC droplets exhibited a fluorescent reflection around the droplets, indicating successful interaction. We anticipate that this simple, low-cost, and label-free optical probe technology will provide foundational insights into the interactions at the PEI/Tween-20 droplet interfaces. This knowledge is expected to be instrumental in the development of sensors for detecting proteins, diseases, and pathogens.

2. Experimental

2.1 Materials and methods

Nematic liquid crystal E7 with an isotropic temperature of 59 °C was obtained from Merck. PEI with a concentration of 50 wt%, and glutaraldehyde (GA) at 25 wt% were procured. Polysorbate 20, commonly known as Tween 20, along with hexadecane, were

supplied by Sigma-Aldrich. Sodium borohydride ($NaBH_4$) was purchased from SRL Chemical Company, India. The anti-beta amyloid-1–16 antibody (Cat. #803001) was acquired from BioLegend Company, while the amyloid-beta protein fragment 1–42 of Human origin was sourced from Genscript. The secondary antibody, anti-mouse IgG(H + L) F(ab′)2 (Product #SAB4600387), was also procured from Sigma-Aldrich. PBS, 1X with a pH of 7.4 was prepared in our laboratory. The pH of the PBS solution was consistently maintained at 7.4 for all measurements. Throughout the experiment, solutions were prepared using ultrapure water obtained *via* Milli-Q purification. All materials were used as received, without any additional purification steps.

2.2 Characterizations

To analyze the director configuration of the LC within the droplets and to capture textural images of these droplets over time, a POM (Olympus BX53, USA) was employed in transmission mode. This microscope was equipped with a CCD camera (Micropublisher RTV 5.0, Imaging), which facilitated observations both with and without crossed polarizers. Additionally, a fluorescence microscope (Olympus IX 73 Inverted microscope) was utilized to observe the immunobinding of the secondary antibody to the antibody–antigen complex on the surface of the LC droplets. This setup allowed for a detailed examination of the interactions and changes occurring within and on the surfaces of the LC droplets.

2.3 Preparation of antibody/antigen solutions

Antibody Aβ1–16, at a concentration of 1 mg mL^{-1}, was acquired from BioLegend. This solution was stored at a temperature range of 2–4 °C. A stock solution of Aβ1–42 was formulated using PBS buffer solution. To attain the necessary final concentration, both the antigen Aβ1–42 and the antibody Aβ1–16 stock solutions were diluted with PBS buffer. Concurrently, the antibody Aβ1–16 and the antigen solution were utilized in an immunobinding reaction. This reaction occurs on the surfaces of LC droplets, a process integral to the early detection of AD.

2.4 Preparation of LC droplets

E7 was combined with hexadecane, constituting 3% w/w as a hydrophobe, and mixed for 10 minutes. This blend of E7 and hexadecane was then incorporated at a 1 : 20 ratio with DI water, which contained 1 wt% PEI and 0.05 wt% Tween-20. The resulting mixture was agitated for 10 minutes at 200 rpm using a Vortex2 Genie mixer from Scientific Industries. After stirring, the mixture was left undisturbed for 4 hours to allow the LC droplets to settle. Subsequently, the aqueous layer was decanted, yielding LC droplets in a 1 : 4 ratio (E7/DI water). These LC microdroplets were stored in a PBS solution, and prepped for binding with anti-β-amyloid 1–16, to facilitate the study of their interactions with the β-amyloid 1–42 peptide in PBS on the LC droplet surface. The orientation of E7 molecules within the LC microdroplets was examined using POM. Our findings demonstrate that varying concentrations of Tween-20 (0.2 wt%, 0.1 wt%, 0.05 wt%) in a 1 wt% PEI solution impact the LC droplets' structure. Under a polarizing optical microscope, all concentrations of Tween-20 coated LC droplets exhibited a radial structure. Among these, the combination of 1 wt% PEI and 0.05 wt% Tween-20 was selected for coating the LC droplets, as depicted in Fig. 1. This composition was also chosen to minimize the incubation time required for configuration changes in the immunoassay of antigen and antibody on the LC droplet surfaces.

2.5 Effect of GA on the LC droplets

Around 100 μL of PBS solution was mixed with 20 μL of a solution containing LC droplets and 4 μL of glutaraldehyde (GA) at a concentration of 0.1 wt%. This emulsion was then incubated for various time intervals: 0 minutes, 5 minutes, 15 minutes, 30 minutes, 1 hour, 4 hours, and 12 hours. The GA solution was prepared using a buffer with a concentration of 0.1 wt% for both GA and $NaBH_4$, ensuring the concentration of $NaBH_4$ did not exceed 150 mM (for the 4 μL solution) to prevent instability and aggregation. Following the reaction, the LC droplets were rinsed twice with PBS buffer to remove any residual GA solution from their surface. Subsequently, the droplets were soaked in 500 μL of PBS–T20 buffer for 15 minutes. This step was essential for both the stabilization of the droplets and preparing them for image analysis.

2.6 Immobilization of antibody on the LC droplets

To eliminate any residual GA, the LC droplets were thoroughly rinsed twice with fresh PBS buffer. Following this, the buffer was carefully decanted and replenished to reach a final volume of 250 μL. For antibody immobilization, the LC droplet emulsion was enhanced with 200 μL of PBS buffer solution containing antibody Aβ1–16 at a concentration of 1 μg mL^{-1}, and this mixture was incubated for 1 hour. After incubation, these LC droplets, now referred to as anti Aβ1–16-LC droplets, underwent a rinsing process with PBS–T20 buffer to remove any unbound antibody. The final step involved immersing the antibody Aβ1–16 decorated LC droplets in PBS solution, concluding the preparation after the 1 hour incubation period.

2.7 Immunobinding experiments

The LC droplets, with immobilized antibodies, were submerged in a 100 μL solution of Aβ1–42 antigen for three hours. During this period, we noted the onset of structural changes in the LC droplets. These changes were closely monitored and analyzed using a POM. For detailed observation, a 2 μL sample of the protein (antibody Aβ1–16)-decorated LC droplet solution was carefully placed on a clean glass slide and examined under a microscope. This process allowed us to observe the secondary antibody's binding with the antibody–antigen complex on the surface of the LC droplets, using a fluorescence microscope for enhanced visualization. In our experiments, we measured the average size of the LC droplets to be between 60 to 85 μm.

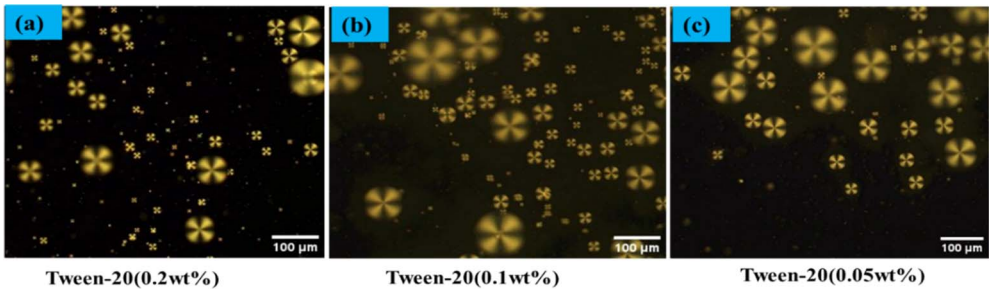

Fig. 1 Polarized optical microscope images of LC droplets coated Tween 20 (a) 0.2 wt%, (b) 0.1 wt%, (c) 0.05 wt%.

3. Results

3.1 Optical textural studies of LC droplets with PEI/Tween-20

In our study of the optical textures of LC droplets coated with PEI (1 wt%) and varying concentrations of Tween 20 (0.05 wt%, 0.1 wt%, 0.2 wt%), as observed under POM a distinctive single defect point at the center as illustrated in Fig. 1. This specific configuration arises when the LC molecules at the droplet interface orient themselves perpendicularly to the droplet surfaces. Upon examining the birefringence of these LC droplets under crossed polarizers, we observed a fan-like or radial structure, particularly in droplets coated with PEI/Tween 20. This phenomenon is attributed to the amphiphilic properties of Tween 20, which allows it to permeate through the PEI layer and accumulate on the surface of the LC droplets.[53] The presence of Tween 20 significantly influences the orientation of the LC within the droplets, as shown in Fig. 1. In a similar manner, coating with SDS (Sodium Dodecyl Sulphate) can achieve radial orientation anchoring of the LC droplets.

A specific concentration of surfactants were selected in the aqueous solution, namely PEI at 1 wt% and Tween 20 at 0.05 wt%, to achieve the radial orientation of LC droplets. It was observed that increasing the concentration of Tween 20 beyond 0.05 wt% necessitates a higher amount of antigen to trigger the transition of LC droplet configuration from radial to bipolar, owing to the surface anchoring properties of the LC droplets. Consequently, Tween 20 at 0.05 wt% was identified as the optimal concentration. In this setup, PEI plays a crucial role in facilitating the attachment of antibodies on the surfaces of the LC droplets.

3.2 Effect of GA on the orientation of LC droplets

To immobilize anti Aβ1–16 on the surface of LC droplets, PEI/Tween 20 coated LC droplets were functionalized with GA. This process introduced aldehyde groups that facilitated the attachment of the protein (anti Aβ1–16) to the surface of the LC droplets. Fig. 2 illustrates the impact of GA on LC droplets over time. Notably, even after 12 hours, the droplets maintained a radial configuration when the concentration of GA was set at 0.1 wt%, as depicted in Fig. 2. A relatively lower concentration of GA was determined, specifically 0.1 wt%, is optimal and should be applied for a duration of 15 minutes to achieve effective immobilization of GA on the surface of the LC droplets.

3.3 Effect of anti-body protein concentration on LC droplets

The radial configuration of the LC (E7) droplets is stabilized by the presence of PEI/Tween 20, with Tween 20 particularly influencing the configuration to a radial form and controlling interactions at the interfaces of the LC droplets. To validate the target-specific binding affinity to LC droplets, we introduced a GA solution into the LC microdroplets. This step was crucial for immobilizing anti Aβ1–16 on the surfaces of the LC droplets, enabling them to interact with the conjugate antigen Aβ1–42 on their surfaces. The presence of aldehyde groups ensures that anti Aβ1–16 is effectively bound to the surfaces of the LC droplets. It's important to note that the binding of anti Aβ1–16 on the surfaces of the LC droplets did not induce any configurational changes on the surfaces of the LC microdroplets. This observation is corroborated by Fig. 2, which displays the textures of GA, and Fig. 3, which shows LC droplets immobilized with anti Aβ1–16. There have been no structural changes observed in both figures (Fig. 2 and 3), indicating the stability of the LC droplets' configuration post-immobilization.

In our study, the impact of different incubation times (1 hour, 3 hours, and 12 hours) were examined on the LC droplets when interacting with antibodies, as depicted in Fig. 4. Remarkably, the LC droplets showed no configurational

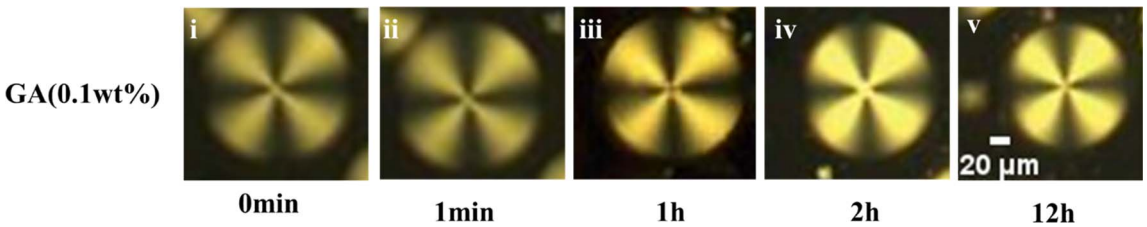

Fig. 2 Effect of GA with respect incubation times on LC droplets under Polarizing Optical Microscope (POM).

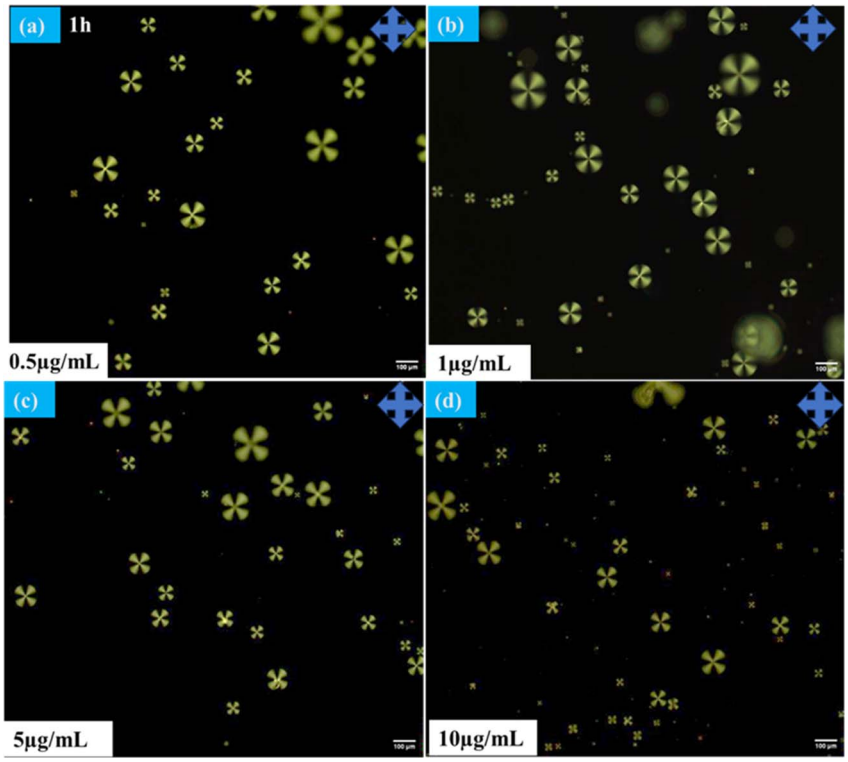

Fig. 3 Polarizing optical microscope images of LC microdroplets immobilized with different concentration anti Aβ1–16 with incubation time for 1 h (a) 0.5 μg mL^{-1}. (b) 1 μg mL^{-1}. (c) 5 μg mL^{-1}. (d) 10 μg mL^{-1}.

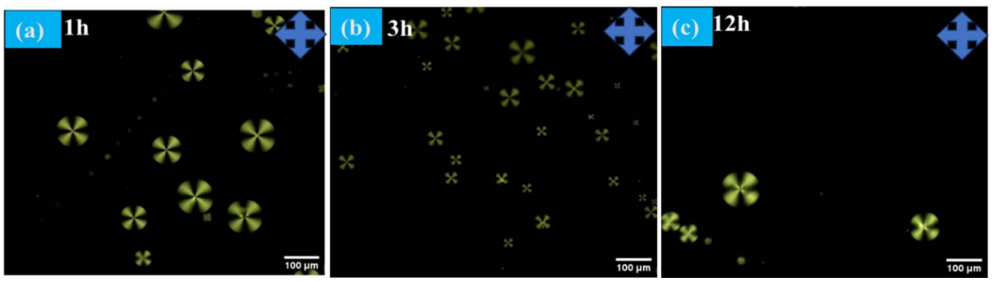

Fig. 4 Polarizing optical microscope images of LC microdroplets anchoring with anti Aβ1–16 with different incubation times (a) 1 h (b) 3 h (c) 12 h at 10 μg mL^{-1} concentration.

changes even after a week. This indicated that the anchoring of the Aβ1–16 antibody did not significantly alter the orientation of the LC droplets, possibly due to weak interaction forces between anti Aβ1–16 and the LC droplets. The attachment of anti Aβ1–16 to the LC microdroplets resulted in symmetrical and weak interaction forces around the nematic liquid droplets. These forces were insufficient to change the orientation of the LC droplets. Furthermore, different concentrations of anti Aβ1–16 were immobilized and observed their behaviour under Polarizing Optical Microscope (POM) with a 1 hour incubation period, as shown in Fig. 3. At higher concentrations, no configurational transition was found in the LC droplets (up to 10 μg mL^{-1}). Based on these observations, the antibody concentration was optimized to be 1 μg mL^{-1}, which showed greater sensitivity compared to other concentrations. This was confirmed by adding varying concentrations of Aβ1–42 peptide (ranging from 22.5–112.5 μM) and noting the structural changes from radial to bipolar configuration. It was also noted that increasing the concentration of antibody Aβ1–16 resulted in the formation of a thicker colloidal layer around the droplets, leading to reduced sensitivity towards the conjugate antigen Aβ1–42 peptide.[48]

3.4 Effect of concentration of Aβ1–42 on LC droplets

The lowest concentration of Aβ1–42 required to change the orientation of immobilized LC droplets from radial to bipolar configuration within 12 h (at an optimized concentration of antibody to be immobilized on LC droplets) is termed as the detection limit (LOD). In this context, determining the optimal antibody concentration is crucial to maintaining the radial

orientation of LC droplets. Our studies led to the identification of this optimum antibody concentration for LC droplets. The LC droplets exhibited a stable radial orientation uniformly across all samples. Even when the antibody concentration was increased, no structural changes were observed under POM, even after a period of 7 days. This led to the conclusion that an excess amount of antibody immobilized on LC droplets does not alter their orientation, even at high concentrations and with extended incubation times. In other words, higher antibody levels (up to 10 μg mL^{-1}) do not disrupt the alignment of the LC droplets.

Our main objective was to determine the optimal antibody concentration for LC droplet surface immobilization. For this purpose, amyloid beta 1–42 antigen solution was introduced into the system with immobilized antibodies on LC droplet surfaces. The sensitivity of the LC droplets was found to be dramatically reduced when Aβ1–16 was anchored onto the LC microdroplets at an antibody concentration of 5 μg mL^{-1}. The antigen Aβ1–42 has interacted with different concentrations of anchor anti Aβ1–16 on the LC droplets surface. Subsequently, incubated the Aβ1–42 antigen up to 12 hours at a concentration of 67.5 μM. The imaging of these samples at various time intervals revealed insightful data, as shown in Fig. 5, pertaining to the interaction dynamics between the LC droplets and the Aβ1–42 antigen. The impact of the antibody on the anchoring of LC droplets was found to be negligible. Our studies to evaluate the impact of antibodies on LC droplets are shown in Fig. 4. Consequently, it was determined that the optimum concentration of the antibody, when interacting with various peptide solutions, induces orientational changes detectable by the LC-based biosensor. This interaction does not adversely affect the anchoring properties of the LC droplets, allowing for accurate and stable biosensing capabilities.

At low peptide concentrations, no structural transition of LC droplets was observed, as the amount of anti Aβ1–16 capturing Aβ1–42 was too low. This was evident from observations under a Polarizing Optical Microscope (POM), as shown in Fig. 6, where at a peptide concentration of 22.5 μM, the effect was minimal. However, as the concentration of the peptide Aβ1–42 increased, more Aβ1–42 was captured by anti Aβ1–16. This increase in Aβ1–42 led to a higher number of immunocomplexes forming between the antibody and antigen, which in turn caused orientational changes in the LC droplets, as demonstrated in Fig. 6. These changes in configuration were significant for understanding the relationship between peptide concentration and antibody concentration, particularly in maintaining the homeotropic radial orientation of LC droplets.

After applying a coating of PEI/Tween 20 to the droplets, the minimum effective concentration of antibody was determined. It was observed that within 3 hours, a transition in configuration could be detected using a polarizing optical microscope. The quantity of Aβ1–16 was adjusted to induce a transition in the LC droplets' configuration from radial to bipolar with a smaller amount of antigen. Specifically, at concentrations below 67.5 μM, only a limited number of droplets exhibited this transition. This discovery confirms the sensitivity of our coated droplets, especially at an optimized concentration of 1 μg mL^{-1} anti Aβ1–16, in comparison to higher concentrations. The transition from radial to bipolar configurations within 3 hours indicates the potential use of LC droplets in the early detection of AD.

Next, we focused on the impact of various parameters, such as the immobilization of the antibody on LC droplets, the concentration of antigen Aβ1–42, and the LOD. These findings are illustrated in Fig. 7(a). Concentration-dependent incubation time has been explored to determine when LC droplets begin to respond after the addition of antigen Aβ1–42 to droplets with immobilized antibody Aβ1–16 at concentrations of 0.5, 1, and 5 μg mL^{-1}. Our observations revealed that an increase in the concentration of antibody immobilized on LC droplets led to a decreased sensitivity in the droplet's response to configurational changes. Conversely, lowering the concentration of antigen Aβ1–42 reduced the sensitivity of the LC droplets response. This decrease in sensitivity is attributed to the fewer antigen Aβ1–42 molecules available, resulting in less immunoreaction between the antibody and antigen, and subsequently, no change in the LC droplets configuration during a 12 hours incubation period. Within a 12 hours incubation, there is no structural change of LC droplets from radial to bipolar, indicating an immunobinding reaction between the

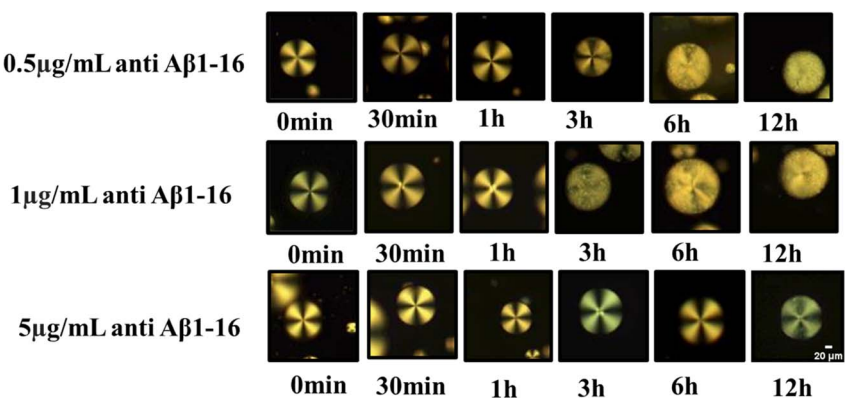

Fig. 5 Polarized optical microscope images of LC droplets of different concentrations of antibody (anti Aβ1–16) at particular concentration antigen Aβ1–42 at 67.5 μM.

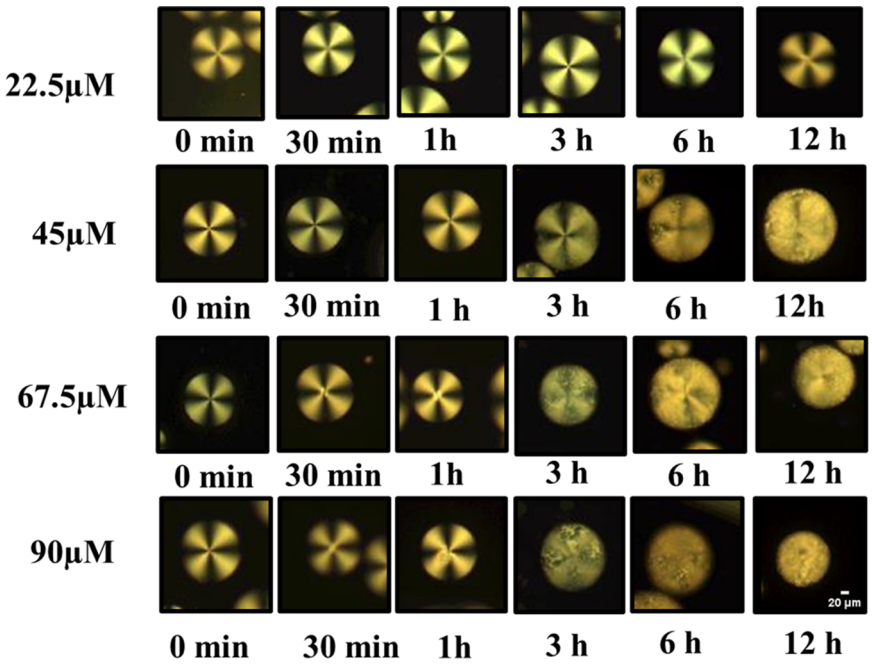

Fig. 6 Polarized optical microscope images of LC droplets of different concentrations of antibody (anti Aβ1–16) at particular concentration antigen Aβ1–42 at 67.5 μM.

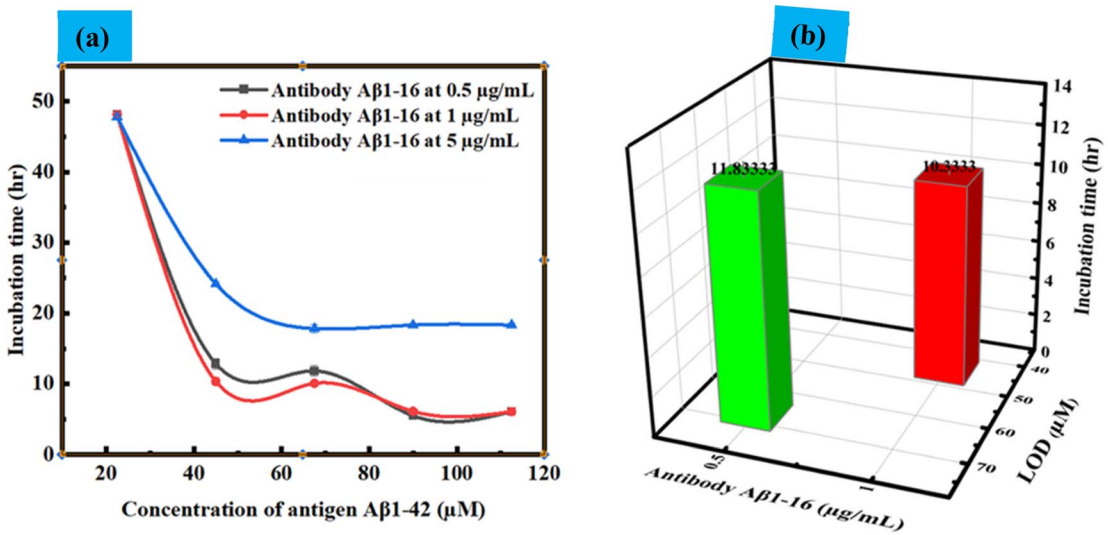

Fig. 7 (a) and (b) Incubation time values *vs.* concentration of antigen Aβ1–42 at particular concentration of antibody Aβ1–16 at 0.5 μg mL^{-1}, 1 μg mL^{-1} and 5 μg mL^{-1} with error bar. (b) Detection limit and incubation time at LOD (up to 12 h).

antibody and antigen. This change was more pronounced when the concentration of antibody immobilized on the LC droplets was increased from 0.5 μg mL^{-1} to 1 μg mL^{-1}. The incubation time for PEI/Tween 20 coated LC droplets varied from 11.8 h to 10.3 h for LOD, with no configuration transition observed for antigen Aβ1–42 concentrations below 45 μM within a 12 hours period at an immobilized antibody concentration of 1 μg mL^{-1}. At a 5 μg mL^{-1} antibody concentration, no configurational changes from radial to bipolar were observed within 12 hours; changes were only noted beyond this period. This could be due to the formation of a thick antibody layer around the droplets, rendering the concentration of antigen Aβ1–42 insufficient to alter the orientation of the LC droplets. In summary, the concentration of immobilized antibody, LOD, and the incubation time at LOD, which correlate to the configurational changes from radial to bipolar, are detailed in Fig. 7(b). The variation in detection limits and sensitivity for antigen Aβ1–42 can be linked to the differing interactions between the antibody and antigen in the immunoassays conducted on the surfaces of LC droplets. This variability is

primarily influenced by the presence of antibodies on the LC surfaces. When antibodies are immobilized on these surfaces, they facilitate the attachment of antigens, leading to immunoassays occurring directly on the LC surfaces. Therefore, the key factor affecting the detection limits and sensitivity in these assays is the extent and manner of antibody immobilization on the LC droplet surfaces.

3.5 Interaction between the antibody and antigen verified by bipolar orientation of LC droplets through POM analysis

The interaction between the antibody and antigen induces a structural change in the LC droplets, shifting from a radial to a bipolar configuration, as observed under a polarizing optical microscope (POM). This structural transition is documented in Fig. 8, which includes POM images of LC droplets after a 12 hours incubation, both with and without a cross polarizer. Scheme 1 provides a schematic representation of how the antibody and antigen attach to the LC droplets, highlighting this molecular interaction and structural transformation.

3.6 Conformation of immunoassay of LC droplets using of secondary antibody

In our quest to gain a deeper insight into this phenomenon a secondary antibody has introduced onto the surfaces of liquid crystal (LC) droplets, maintaining a pH level of 7.4. This was done both in the presence and absence of the immobilized primary antibody Aβ1–16. Our observations, conducted under fluorescence microscopy, unveiled a significant development. The LC droplets exhibited a striking fluorescence emission, an unmistakable sign of the successful attachment of the secondary antibody to the LC droplet surfaces. This attachment coincided with the adoption of a bipolar configuration by the LC droplets, as vividly depicted in Fig. 9(a and b), where both fluorescence and bright-field images are presented.

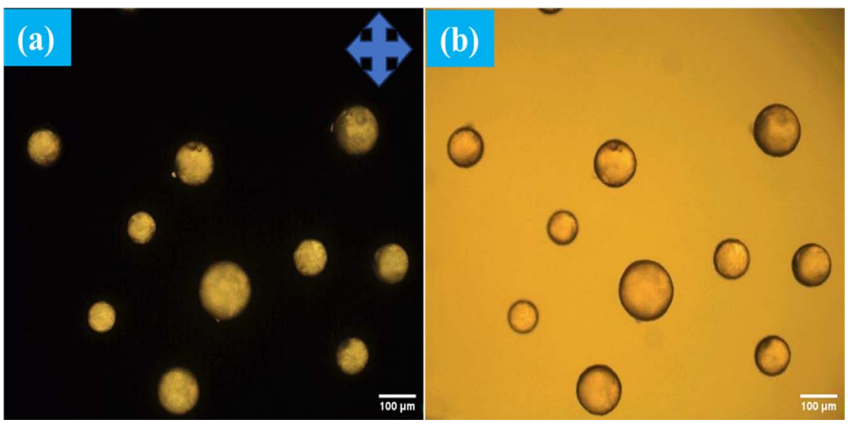

Fig. 8 POM images of immobilized antibody 1 μg mL^{-1} on surfaces of LC droplets at pH 7.4 after addition Aβ1–42 at concentration of 112.5 μM with (a) and without (b) cross polarizer.

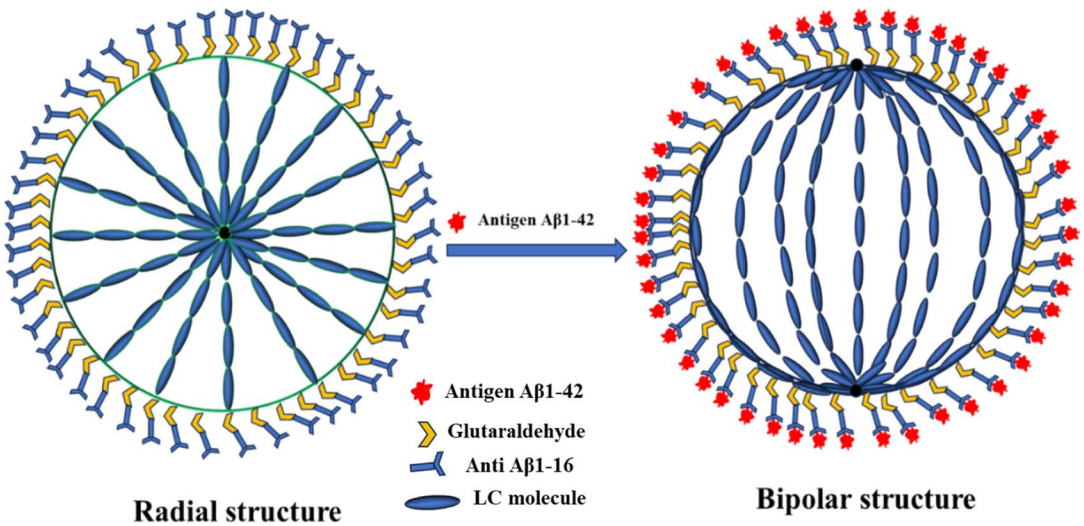

Scheme 1 The schematic representation of the configurational transition from radial to bipolar director configuration of LC immobilized antibody and glutaraldehyde (GA) on the surface's droplets stabilized using PEI/Tween 20, which is caused by the immunobinding reaction between antibody and antigen.

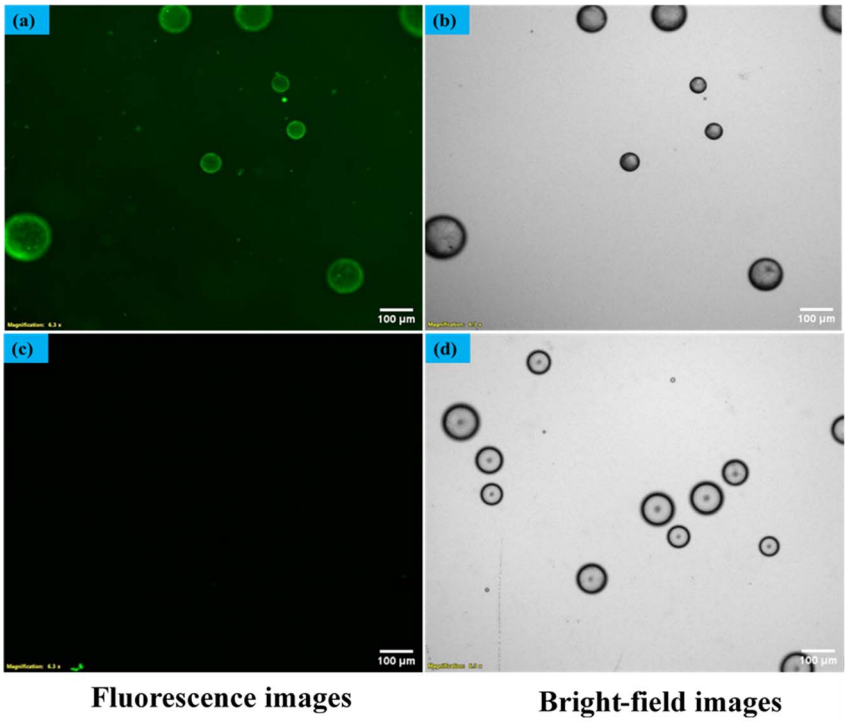

Fig. 9 The LC droplets of fluorescent images (a and c) and bright filed mode images (b and d) by addition of secondary antibody. Where (a and b) images of LC droplets with immunobinding between antibody and antigen (c and d) images of droplets with immunobinding.

Furthermore, this intricate attachment mechanism is meticulously delineated in Scheme 2, elucidating the intricate interaction between the secondary antibody and the LC droplet surfaces.

In stark contrast, LC droplets lacking the immobilized primary antibody showed no fluorescence emission when examined under the fluorescence microscope. This absence of fluorescence indicated the absence of attachment of the secondary antibody. Consequently, it became evident that the attachment of the secondary antibody is contingent upon the preceding immunobinding reaction between the primary antibody and the antigen on the LC droplet surfaces. This fascinating phenomenon is vividly illustrated in Fig. 9(c and d), where fluorescence and bright-field images of the LC droplets in a radial configuration are displayed.

To sum up, the interaction between the antibody immobilized on the LC droplet surfaces and the antigen in an aqueous solution, particularly when the optimum concentration for immobilization on the LC droplets is achieved, induces a profound structural transformation. When the immobilized

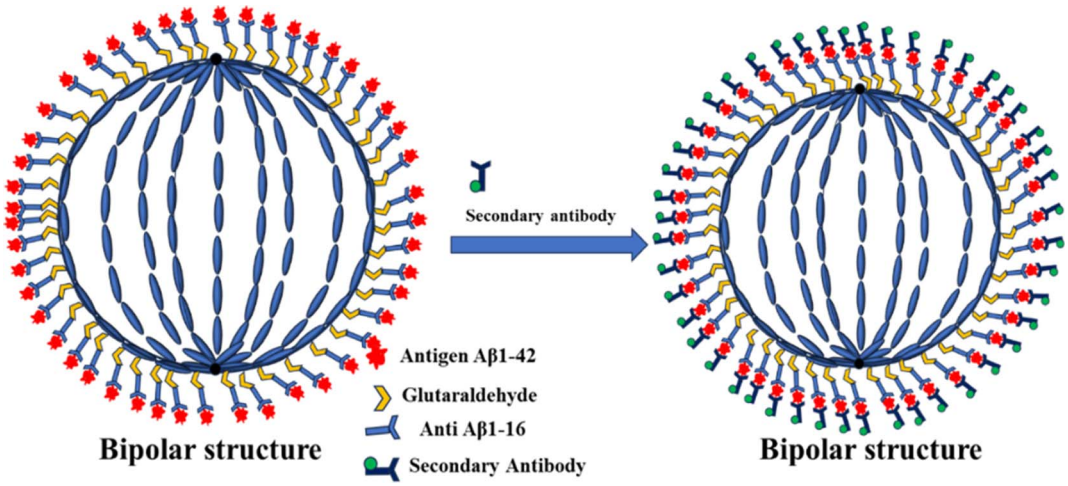

Scheme 2 Schematic representation fluorescence images of LC (E7) droplets stabilized by PEI/Tween-20 and immobilized with anti Aβ1–16, which is the attachment of secondary caused by the immunoassay between antibody to antigen at pH-7.4.

Table 1 Comparison between LC droplets sensing platform and other LC plat form for detection of amyloid beta 1–42

LC martials	Sensing platform	Detection range	Duration of detection	LOD	Reference
Nematic liquid crystal (5CB)	LC–solid interference	100–1000 pg	8–12 min	100 pg	44
Nematic liquid crystal (5CB)	LC–solid interference	1–1000 pg	1.5 h (90 min)	1 pg	43
Nematic liquid crystal (E7)	LC droplets interference	45–112.5 μM	3–12 h	45 μM	This work

LC droplets are exposed to the Aβ1–42 (Aβ1–42 peptide) antigen solution, they undergo a remarkable transition from a radial to a bipolar configuration.

4. Discussion

We have demonstrated that PEI/Tween 20-coated NLC droplets exhibit a radial configuration, as illustrated in Fig. 1. When these liquid crystal droplets were immobilized with antibodies at various concentrations, there were no observable changes in their configuration, as shown in Fig. 3. This lack of change may be attributed to the inability of the antibodies themselves to disrupt the orientation of the liquid crystal molecules, as elaborated upon in Section 3.3.

It is important to note that the optical appearance of LC droplets, when immobilized with antibodies at low antigen concentrations, continues to display a radially-anchored configuration under crossed polarizers. This configuration depends on the relative positions of the focus plane and the droplet center. Notably, the transition from a radial to a bipolar arrangement was solely detected in droplets during the immunobinding reaction occurring on the surfaces of the LC droplets.

Fig. 6 (Aβ1–42 at 22.5 μM) demonstrates that LC droplets at the interfaces maintain a radial orientation when they are not in close proximity to the immunobinding reaction. In contrast, LC droplets in the immobilization of antibodies (without adding antigen) display a radial configuration, as shown in Fig. 4. To confirm that the change in orientation of the nematic LC droplets is due to the presence of the immunobinding reaction and no other factors, we have conducted separate experiments involving the addition of antibodies Aβ1–16 and Aβ1–42 antigens at varying concentrations and incubation times of up to 12 hours. These experiments did not result in LC droplets exhibiting a bipolar configuration or any measurable change in orientation compared to what was observed in the antibody–antigen immunoassay.

This confirms that the orientation change in LC droplets is indeed due to the presence of the immunobinding reaction on the surfaces of the liquid crystal droplets. We further investigated the orientational behavior of NLC droplets at different antibody concentrations with a specific antigen concentration, as shown in Fig. 5. POM images (without crossed polarizers in bright field mode) of NLC droplets surrounded by antigen (Fig. 9(c and d)) reveal that these NLC droplets do not exhibit a bipolar configuration, and their orientation remains largely unchanged after incubation with antigen for 12 hours. Thus, the transition from a radial to a bipolar configuration of LC droplets is a result of the immunobinding reaction between antibodies and antigens on the surfaces of the LC droplets, as illustrated in Fig. 8 and Scheme 1.

We also demonstrated the ability of LC emulsions coated with PEI/Tween 20 and immobilized with antibody Aβ1–16 on their surfaces to detect amyloid beta 1–42 antigen. This transition to a bipolar configuration corroborates the impact of the immunobinding reaction between antibodies and antigens on LC surfaces. Our incubation duration for the antibody is 1 hour, which is notably shorter than the typical incubation time of 8 hours used by other LC droplets and LC-based biosensors for amyloid beta 1–42 detection.[43] In a different biosensor developed by our lab, the response time has been dependent on droplet size and protein content.[51,52] This emphasizes the importance of optimization processes in biosensor development.

Our prior studies have similarly revealed structural changes from homeotropic to planar configurations in cholesteric liquid crystal droplets when detecting BSA and bile acid.[51,52] Additionally, Table 1 provides a comparison with other LC-based biosensors for the detection of amyloid beta 1–42. We are identifying amyloid beta 1–42 in the flat geometry in terms of intensities. In this case, we used LC droplets with a limit of detection (LOD) of 45 μM.

In addition, we carried out conformational studies on immunobinding LC droplets by incubating them with a secondary fluorescently labeled antibody solution at 5 μg mL^{-1} for 1 hour. After this incubation period, the immunobinding LC droplets were rinsed with a PBS solution to remove any excess unattached secondary antibodies from their surfaces. When we examined these LC droplets under a fluorescence microscope, incubated with and without immunobinding on the surfaces while adding secondary antibodies, as shown in Fig. 9 and Scheme 2, we obtained further confirmation that the immunoreaction occurs on the surfaces of LC droplets, as the secondary antibodies were only attached to the LC droplet surfaces. This method holds promise for screening a large number of samples and lays the groundwork for developing a rapid and sensitive screening assay for disease biomarkers and pathogens, based on the configurational changes of LC droplets.

5. Conclusions

Our investigation has successfully demonstrated that NLC droplets can serve dual roles as a host matrix and a sensing platform for the detection of AD biomarker, specifically the Aβ1–42 peptide. To achieve this, we meticulously coated the LC droplets with a tailored composition of PEI at 1 wt% and Tween 20 at 0.05 wt%. This bespoke coating plays a pivotal role in establishing homeotropic anchoring, which is crucial for

inducing a radial configuration within the droplets. We further enhanced the system by immobilizing anti Aβ1–16 antibodies on the surface of the LC droplets, employing GA as a cross-linking agent. This sophisticated enhancement considerably augments the droplets' sensitivity in detecting the Aβ1–42 antigen. The cornerstone of this innovative detection methodology lies in the formation of an immunocomplex, arising from the interaction between the antibodies and antigens on the LC droplet surface. This immunocomplex disrupts the initial radial alignment of the LC droplets, instigating a transformative shift to a planar (bipolar) alignment. This critical transition is efficiently observable and analysable using POM. Our research further unveils that the alignment of LC droplets, governed by the synergistic interaction of PEI and Tween 20 at the LC–water interface, can be adeptly employed as an optical signal. This novel approach is promising not only for AD biomarkers but also as a versatile, adaptable tool in the broader spectrum of disease diagnostics and biomarker discovery, underscoring its extensive potential in medical research and clinical applications.

Data availability

The data will be available from the corresponding author on reasonable request.

Conflicts of interest

The authors declare that they have no known competing financial interests or personal relationships that could have appeared to influence the work reported in this paper.

Author contributions

SRP: investigation, formal analysis, data curation, writing – original draft, visualization. RSP: data curation, writing – original draft, visualization. RK: writing – original draft, visualization. KC: data curation, writing – original draft, visualization, supervision, funding acquisition. MV: data curation: supervision. JV: conceptualization, methodology, validation, resources, writing – original draft, visualization, supervision, project administration, funding acquisition.

Acknowledgements

The authors would like to express their gratitude to the Department of Biotechnology in New Delhi, India, for their financial assistance, which came in the form of Research Grant No. BT/PR35841/MED/32/745/2020. The authors of this paper express thanks to Department of Physics and the Central Research Instrumentation Facility (CRIF) at NIT Warangal for providing their research facilities.

References

1 H. F. Han, H. C. Yen, H. C. Wu, H. Y. Tan, W. Xu, H. S. Jiang, P. J. Tsai, K. Qian, Y. C. Wu and C. C. Chen, *ACS Appl. Mater. Interfaces*, 2021, **13**, 57036–57042.
2 J. H. Kang, M. Korecka, M. J. Figurski, J. B. Toledo, K. Blennow, H. Zetterberg, T. Waligorska, M. Brylska, L. Fields, N. Shah, H. Soares, R. A. Dean, H. Vanderstichele, R. C. Petersen, P. S. Aisen, A. J. Saykin, M. W. Weiner, J. Q. Trojanowski and L. M. Shaw, *Alzheimer's Dementia*, 2015, **11**, 772–791.
3 K. Blennow, *Neurol. Ther.*, 2017, **6**, 15–24.
4 C. M. Startin, N. J. Ashton, S. Hamburg, R. Hithersay, F. K. Wiseman, K. Y. Mok, J. Hardy, A. Lleó, S. Lovestone, L. Parnetti, H. Zetterberg, A. Hye, E. Fisher, D. Nizetic, V. Tybulewicz, A. Karmiloff-Smith, T. Al-Janabi, D. Zhang and A. Strydom, *Alzheimer's Res. Ther.*, 2019, **11**, 1–12.
5 K. Kim, M. J. Kim, D. W. Kim, S. Y. Kim, S. Park and C. B. Park, *Nat. Commun.*, 2020, **11**, 1–9.
6 S. Janelidze, N. Mattsson, S. Palmqvist, R. Smith, T. G. Beach, G. E. Serrano, X. Chai, N. K. Proctor, U. Eichenlaub, H. Zetterberg, K. Blennow, E. M. Reiman, E. Stomrud, J. L. Dage and O. Hansson, *Nat. Med.*, 2020, **26**, 379–386.
7 Z. Huang, M. Li, L. Zhang and Y. Liu, *Front. Bioeng. Biotechnol.*, 2022, **10**, 1–9.
8 U. C. Muller and H. Zheng, *Cold Spring Harbor Perspect. Med.*, 2012, **2**, a006288.
9 M. Ammar, C. Smadja, L. Giang Thi Phuong, M. Azzouz, J. Vigneron, A. Etcheberry, M. Taverna and E. Dufour-Gergam, *Biosens. Bioelectron.*, 2013, **40**, 329–335.
10 J.-W. Choi, A. T. M. K. Islam, J.-H. Lee, J. M. Song and B.-K. Oh, *J. Nanosci. Nanotechnol.*, 2011, **11**, 4200–4204.
11 T. E. Golde, C. B. Eckman and S. G. Younkin, *Biochim. Biophys. Acta, Mol. Basis Dis.*, 2000, **1502**, 172–187.
12 C. Haass and D. J. Selkoe, *Nat. Rev. Mol. Cell Biol.*, 2007, **8**, 101–112.
13 M. A. Findeis, *Pharmacol. Ther.*, 2007, **116**, 266–286.
14 A. Peric and W. Annaert, *Acta Neuropathol.*, 2015, **129**, 363–381.
15 D. R. Thal, J. Walter, T. C. Saido and M. Fändrich, *Acta Neuropathol.*, 2015, **129**, 167–182.
16 P. C. May, B. A. Willis, S. L. Lowe, R. A. Dean, S. A. Monk, P. J. Cocke, J. E. Audia, L. N. Boggs, A. R. Borders, R. A. Brier, D. O. Calligaro, T. A. Day, L. Ereshefsky, J. A. Erickson, H. Gevorkyan, C. R. Gonzales, D. E. James, S. S. Jhee, S. F. Komjathy, L. Li, T. D. Lindstrom, B. M. Mathes, F. Martényi, S. M. Sheehan, S. L. Stout, D. E. Timm, G. M. Vaught, B. M. Watson, L. L. Winneroski, Z. Yang and D. J. Mergott, *J. Neurosci.*, 2015, **35**, 1199–1210.
17 Z. Luo, H. Xu, L. Liu, T. Y. Ohulchanskyy and J. Qu, *Biosensors*, 2021, **11**, 255.
18 N. Kaneko, A. Nakamura, Y. Washimi, T. Kato, T. Sakurai, Y. Arahata, M. Bundo, A. Takeda, S. Niida, K. Ito, K. Toba, K. Tanaka and K. Yanagisawa, *Proc. Jpn. Acad., Ser. B*, 2014, **90**, 353–364.
19 Y. I. Kostyukevich, A. S. Kononikhin, M. I. Indeykina, I. A. Popov, K. V. Bocharov, A. I. Spassky, S. A. Kozin, A. A. Makarov and E. N. Nikolaev, *Mol. Biol.*, 2017, **51**, 627–632.
20 L. Liu, N. Xia, J. Zhang, W. Mao, Y. Wu and X. Ge, *Anal. Methods*, 2015, **7**, 8727–8732.

21 J. S. Park, H. J. Kim, J. H. Lee, J. H. Park, J. Kim, K. S. Hwang and B. C. Lee, *Sensors*, 2018, **18**, 426.
22 H. Ke, H. Sha, Y. Wang, W. Guo, X. Zhang, Z. Wang, C. Huang and N. Jia, *Biosens. Bioelectron.*, 2018, **100**, 266–273.
23 J. X. Wang, Y. Zhuo, Y. Zhou, H. J. Wang, R. Yuan and Y. Q. Chai, *ACS Appl. Mater. Interfaces*, 2016, **8**, 12968–12975.
24 X. Liu, Z. Wang, F. Yin, Y. Liu, N. Qin, Y. Nakamura, F. Shahidi, C. Yu, D. Zhou and B. Zhu, *Mar. Drugs*, 2019, **17**, 1–14.
25 A. Garcia-Leis and S. Sanchez-Cortes, *ACS Appl. Nano Mater.*, 2021, **4**, 3565–3575.
26 A. Kaushik, R. D. Jayant, S. Tiwari, A. Vashist and M. Nair, *Biosens. Bioelectron.*, 2016, **80**, 273–287.
27 S. Y. Yang, M. J. Chiu, T. F. Chen and H. E. Horng, *Neurol. Ther.*, 2017, **6**, 37–56.
28 L. Song, D. R. Lachno, D. Hanlon, A. Shepro, A. Jeromin, D. Gemani, J. A. Talbot, M. M. Racke, J. L. Dage and R. A. Dean, *Alzheimer's Res. Ther.*, 2016, **8**, 1–15.
29 I. Verma, S. Sidiq and S. K. Pal, *Liq. Cryst.*, 2019, **46**, 1318–1326.
30 R. R. Shah and N. L. Abbott, *Science*, 2001, **293**, 1296–1299.
31 T. Govindaraju, P. J. Bertics, R. T. Raines and N. L. Abbott, *J. Am. Chem. Soc.*, 2007, **129**, 11223–11231.
32 V. K. Gupta, J. J. Skaife, T. B. Dubrovsky and N. L. Abbott, *Science*, 1998, **279**, 2077–2080.
33 A. D. Abbasi, Z. Hussain and K.-L. Yang, *Molecules*, 2021, **26**, 2893.
34 Y.-C. Hsiao, Y.-C. Sung, M.-J. Lee and W. Lee, *Biomed. Opt. Express*, 2015, **6**, 5033.
35 J. M. Brake, A. D. Mezera and N. L. Abbott, *Langmuir*, 2003, **19**, 6436–6442.
36 C. Zafiu, Z. Hussain, S. Küpcü, A. Masutani, P. Kilickiran and E. K. Sinner, *Biosens. Bioelectron.*, 2016, **80**, 161–170.
37 S. Sivakumar, K. L. Wark, J. K. Gupta, N. L. Abbott and F. Caruso, *Adv. Funct. Mater.*, 2009, **19**, 2260–2265.
38 D. Hartono, C. Y. Xue, K. L. Yang and L. Y. L. Yung, *Adv. Funct. Mater.*, 2009, **19**, 3574–3579.
39 M. Khan, A. R. Khan, J. H. Shin and S. Y. Park, *Sci. Rep.*, 2016, **6**, 1–11.
40 M. Khan, S. Liu, L. Qi, C. Ma, S. Munir, L. Yu and Q. Hu, *TrAC, Trends Anal. Chem.*, 2021, **144**, 116434.
41 M. C. D. Carter, D. S. Miller, J. Jennings, X. Wang, M. K. Mahanthappa, N. L. Abbott and D. M. Lynn, *Langmuir*, 2015, **31**, 12850–12855.
42 I. Pani, P. Madhu, N. Najiya, A. Aayush, S. Mukhopadhyay and S. K. Pal, *J. Phys. Chem. Lett.*, 2020, **11**, 9012–9018.
43 E. Kemiklioglu, E. B. Tuncgovde and G. Ozsarlak-Sozer, *J. Biosci. Bioeng.*, 2021, **132**, 88–94.
44 H. Sohrabnavi, M. Mohammadimasoudi and H. Hajghassem, *Sens. Actuators, B*, 2024, **401**, 134966.
45 T. Bera and J. Fang, *Langmuir*, 2013, **29**, 387–392.
46 Y. Choi, K. Lee, K. C. Gupta, S. Y. Park and I. K. Kang, *J. Mater. Chem. B*, 2015, **3**, 8659–8669.
47 D. Wang, S. Y. Park and I. K. Kang, *J. Mater. Chem. C*, 2015, **3**, 9038–9047.
48 K. Lee, K. C. Gupta, S. Y. Park and I. K. Kang, *J. Mater. Chem. B*, 2016, **4**, 704–715.
49 Y. Huan, S. J. Park, K. C. Gupta, S. Y. Park and I. K. Kang, *RSC Adv.*, 2017, **7**, 37675–37688.
50 L. Yang, M. Khan and S. Y. Park, *RSC Adv.*, 2015, **5**, 97264–97271.
51 S. Ranjan Pradhan, B. Gollapelli, R. Suguru Pathinti, R. Kandimalla and J. Vallamkondu, *J. Mol. Liq.*, 2023, **386**, 122447.
52 B. Gollapelli, A. K. Tatipamula, S. Dewanjee, R. S. Pathinti and J. Vallamkondu, *J. Mater. Chem. C*, 2021, **9**, 13991–14002.
53 V. J. Aliño, J. Pang and K. L. Yang, *Langmuir*, 2011, **27**, 11784–11789.